International Journal of Innovative Computing, Information and Control
Volume **22**, Number **2**, April **2026**

ICIC International ©2026 ISSN 1349-4198
pp. 335–353

DAS-VSP SEISMIC DATA DENOISING BASED ON A MULTI-SCALE AND CROSS-DENSE RESIDUAL NETWORK

Tie Zhong[1,2], Fanchao Xue[2] and Shiqi Dong[1,2,*]

[1]Key Laboratory of Modern Power System Simulation and Control
and Renewable Energy Technology, Ministry of Education
[2]Department of Communication Engineering
Northeast Electric Power University
No. 169, Changchun Road, Jilin 132012, P. R. China
{ zht; 2202300377 }@neepu.edu.cn; *Corresponding author: 20233186@neepu.edu.cn

Received June 2025; revised September 2025

Abstract. *In recent years, the substantial contamination of distributed acoustic sensing vertical seismic profile (DAS-VSP) records by diverse noise sources poses significant challenges for processes in achieving precise noise suppression and accurately recovering the effective signals, which leads to a low signal-to-noise ratio (SNR) of the DAS-VSP records. The potential of deep learning-based convolutional neural networks (CNNs) has demonstrated notable efficacy in suppressing noisy seismic data. However, traditional CNN-based methods are constrained by fundamental architectural deficiencies, which reduces the effectiveness of CNN-based methods. To address this issue, this paper introduces multi-scale cross-dense residual network (MCDR-Net), a novel architecture integrating cross-dense connections and multi-path hybrid attention mechanisms. The cross-dense framework facilitates multi-scale feature interactions through densely connected residual pathways, enabling simultaneous preservation of high-frequency signal details (such as weak reflections) and low-frequency structural patterns. Complementing this, our hybrid attention mechanism employs parallel channel-spatial adaptive weighting and cross-scale gating operations to dynamically amplify coherent seismic features while suppressing incoherent noise components. Compared with other denoising methods, the corresponding experimental results reveal that MCDR-Net can significantly improve the signal-to-noise ratio, such as over 3 dB increment over U-Net. The outcomes of both synthetic and field DAS-VSP records indicate that the proposed MCDR-Net can achieve effective noise suppression in DAS-VSP data and efficiently restore signals, even under scenarios of ultra-low SNR.*

Keywords: DAS-VSP, Seismic denoising, Convolutional neural network, Seismic data processing, Weak signal recovery, Hybrid attention mechanism

1. **Introduction.** Distributed acoustic sensing (DAS) [1] analyzes phase variations in back scattered light to measure subsurface strain changes caused by seismic wave propagation, offering significant advantages. The distributed acoustic sensing vertical seismic profile (DAS-VSP) technology [2,3] integrates the benefits of DAS, providing superior spatial resolution, high sensitivity, cost-effectiveness, and precision. However, DAS-VSP data acquisition faces some challenges, especially the interference of various background noise, which reduces the signal-to-noise ratio (SNR) of the field data severely, and influence the accuracy of subsequent velocity inversion and imaging processes. Consequently, developing efficient techniques for noise suppression method is crucial.

To address noise contamination in DAS-VSP records, different methods of noise reduction are introduced which can be approximately divided into five distinct categories. The

DOI: 10.24507/ijicic.22.02.335

first comprises traditional methods, including Wiener filtering, median filtering, band-pass filtering (BPF) [4], and f-x deconvolution filter [5]. However, in practical data processing, such methods heavily rely on predefined conditions. When actual scenarios deviate from these assumptions, their performance can degrade significantly. The second category including the time-frequency techniques [6,7], such as S-transform [8], short-time Fourier transform [9], and time-frequency peak filtering (TFPF) [10]. The performance of these methods heavily relies on determination of threshold and separation accuracy of signal and noise. Therefore, these limitations may result in the degeneration when confronted with complicated seismic data suffered with aliasing background noise. The third category comprises the decomposition methods, such as wavelet transform (WT) [11], empirical mode decomposition (EMD) [12,13], and ensemble empirical mode decomposition (EEMD) [14,15]. However, this decomposition may lead to distortion of reconstruction signals or performance degradation. The fourth category includes the methods of sparse transformation [16], such as curve transformation [17], and dictionary learning [18]. However, its performance is extremely sensitive to the threshold parameter in the denoising process, and it is easy to introduce phantom or false structure into the denoising results. The fifth category consists of the denoising methods based on low rank matrix [19], such as principal component analysis (PCA) [20] and robust principal component analysis (RPCA) [21,22]. However, the denoising effect is often poor for data containing strong random noise. Besides the aforementioned categories, numerous techniques such as the Karhunen-Loeve transform (K-L transform) [23] are also extensively employed. Worse still, along with the demand for resource development in complex geological structures, the quality of seismic records has deteriorated significantly. In some cases, the performance of traditional methods is unable to meet the requirements.

In recent years, the rapid evolution of deep learning techniques, particularly convolutional neural networks (CNNs) [24] based noise reduction techniques are introduced, such as the generative adversarial network (GAN) [25], denoising convolutional neural network (DnCNN) [26], the fast and flexible denoising network (FFD-Net) [27], and U-Net [28,29], for handling complex seismic noise. Differing from the conventional techniques, deep learning approaches are capable of effectively diminishing intricate seismic noise adaptively without artificially adjusted parameters. However, the existing denoising networks generally have the defect of single-scale information dependence, which may lead to their lack of robustness and reliability when dealing with highly complex and highly uncertain noise environments. Therefore, how to effectively deal with the uncertainty of the data and the model itself in the process of denoising has become an important research direction in this field. For example, the use of emerging mathematical tools such as Pythagorean Fuzzy Sets provides a new perspective and new method to deal with uncertainty for noise feature description and processing [30]. Hence, this paper primarily focuses on employing a multi-scale architecture of network for information generalization.

Based on the analysis of the aforementioned issue on denoising of DAS-VSP data, we establish a novel denoising network named multi-scale cross-dense residual network (MCDR-Net). The architecture incorporates three fundamental innovations that holistically address key limitations in existing approaches.

1) Dual-branch hierarchical processing with cross-dense connectivity

MCDR-Net incorporates a dual-branch structure to process multi-scale features in parallel. Through dense cross connections between the branches, the network enhances feature reuse capabilities and enables hierarchical noise suppression.

2) Centralized multi-scale fusion with adaptive weighting

A centralized fusion mechanism is developed to integrate multi-level features across varying receptive fields. By adaptively combining shallow-layer texture details and deep-layer semantic information through cross-scale concatenation, this mechanism strengthens feature interaction and optimizes weak signal recovery [31].

3) Hybrid attention-guided feature interconnection

The network incorporates a hybrid attention module that coherently integrates channel and spatial attention mechanisms. This module dynamically recalibrates feature responses to prioritize geophysically meaningful signal components while suppressing incoherent noise.

This framework ensures balanced performance in noise suppression, computational efficiency, and weak signal preservation for DAS-VSP data processing.

2. Theory.

2.1. Noise analysis in DAS-VSP.

Figure 1(a) displays a DAS-VSP record collected from an exploration region in western China. The x- and y-axis represent trace and recording time, respectively. This DAS-VSP record is acquired with temporal sampling rate of 2,500 Hz and receiver spacing of 1 m. As shown in Figure 1(b), the data is significantly affected by strong noise, making it challenging to identify the effective signals. Various types of noise contaminate the signals, including fading noise (marked by the red arrow), random noise (marked by the yellow arrow), horizontal noise (marked by the green arrow), and optical noise (marked by the blue arrow). These types of noise are common in optical measurement systems and can compromise their accuracy and reliability. Meanwhile, we also analyze the spectral properties of the DAS background noise, whose results are shown in Figure 1. Notably, the intense noise represents different features and almost exists across the entire frequency bands. For example, fading noise is typical low-frequency interference, while optical noise has frequency overlap with effective signals, which induces the degraded performance of conventional methods. To enhance system performance, it is essential to thoroughly analyze the sources and characteristics of these noises and develop effective suppression and elimination strategies to ensure the accuracy and reliability of measurement data.

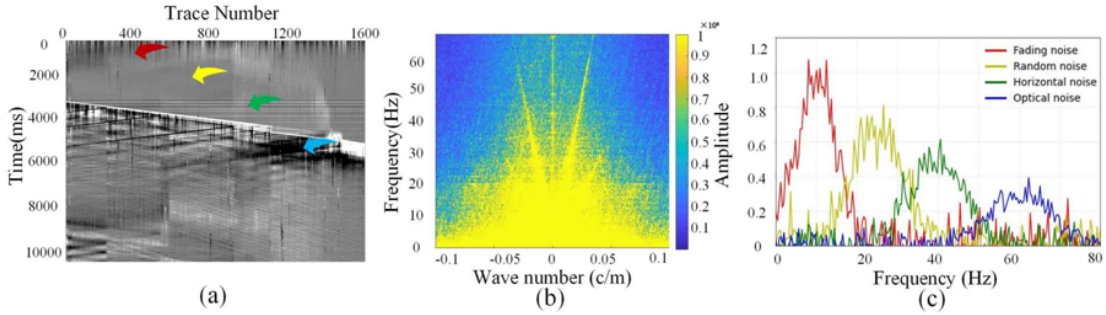

FIGURE 1. Noise analysis in DAS-VSP: (a) DAS-VPS data with several common noises; (b) F-K domain analysis for DAS-VPS data; (c) frequency-amplitude characteristic diagram

2.2. Denoising principles.

Separating clean seismic signals from complex noisy data is the main challenge of processing DAS-VSP records. The clean seismic data containing noise can be mathematically represented as follows:

$$y = x_{clean} + n \tag{1}$$

where y represents the noisy seismic record, which is a superposition of the clean signal x_{clean} and random noise n. To achieve efficient denoising, we propose the MCDR-Net based on the theory of CNNs, which aims to learn a complex nonlinear function that maps a noisy record y to the estimated clean signal x_{est} that is close to a clean signal x_{clean}:

$$x_{est} = F(y; \theta) \tag{2}$$

where the nonlinear mapping relationship F is related to the learnable parameters $\theta = \{\omega, b\}$ of the network, which are continuously optimized through a training process to minimize the difference between the estimated signal x_{est} and the clean signal x_{clean}. ω and b represent the weights and biases, respectively.

In order to optimize θ, a specific loss function is adopted in this study to measure the distances between the x_{est} and the clean signal x_{clean} for making the estimated signal as close as possible to the expected clean signal, and so as to achieve better denoising:

$$l(\theta) = \sum_{k=1}^{K} \|x_{clean} - x_{est}\|^2 / 2K \tag{3}$$

where l represents the loss function, K is the number of samples and $\|\bullet\|$ represents the $L2$ norm.

In practice, we obtain this set of optimal parameters θ_{opt} through minimizing the loss function, and then the trained MCDR-Net model can be deployed to process any untrained noisy records that are not included in the training set. By calculating $F(y_{new}; \theta_{opt})$, we can get an estimated signal x_{new_est} that is close to the clean signal, thus providing a higher quality data for subsequent processing of seismic data.

Based on the above theoretical framework, the denoising process is divided into two stages: training and testing, as shown in Figure 2.

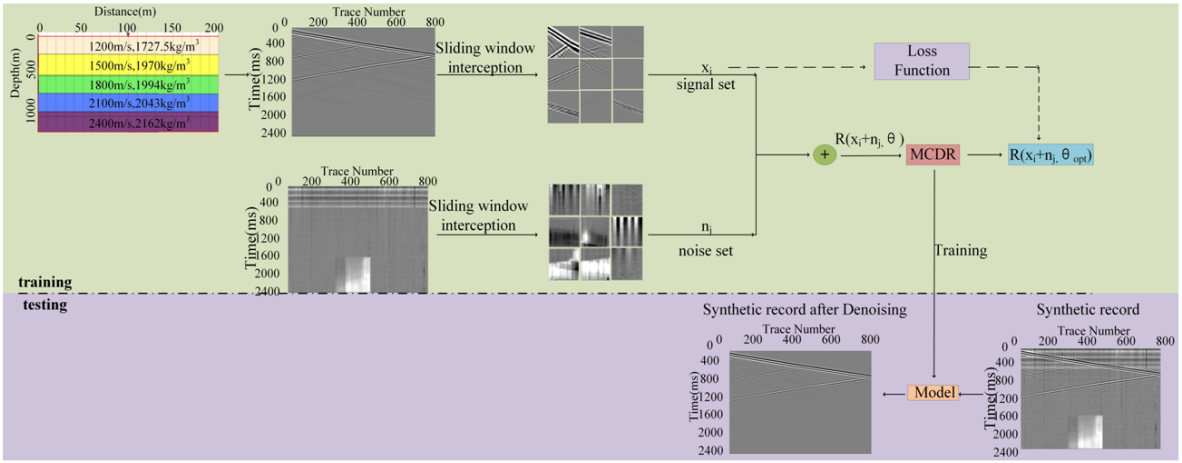

FIGURE 2. Flowchart of the MCDR-Net denoising process

3. **Network Structure.** This paper, based on systematic analysis and comprehensive review of research literature, proposes the development sophisticated deep learning technology for the development of a formidable multi-level convolutional neural network. As shown in Figure 3(a), MCDR-Net comprises a multi-path collaborative processing structure: the upper branch extracts multi-resolution features according to the spatial resolution changes through multi-resolution parallel convolution module (MRPC) (Figure 3(b)). The lower branch expands the receptive field to capture multi-scale information

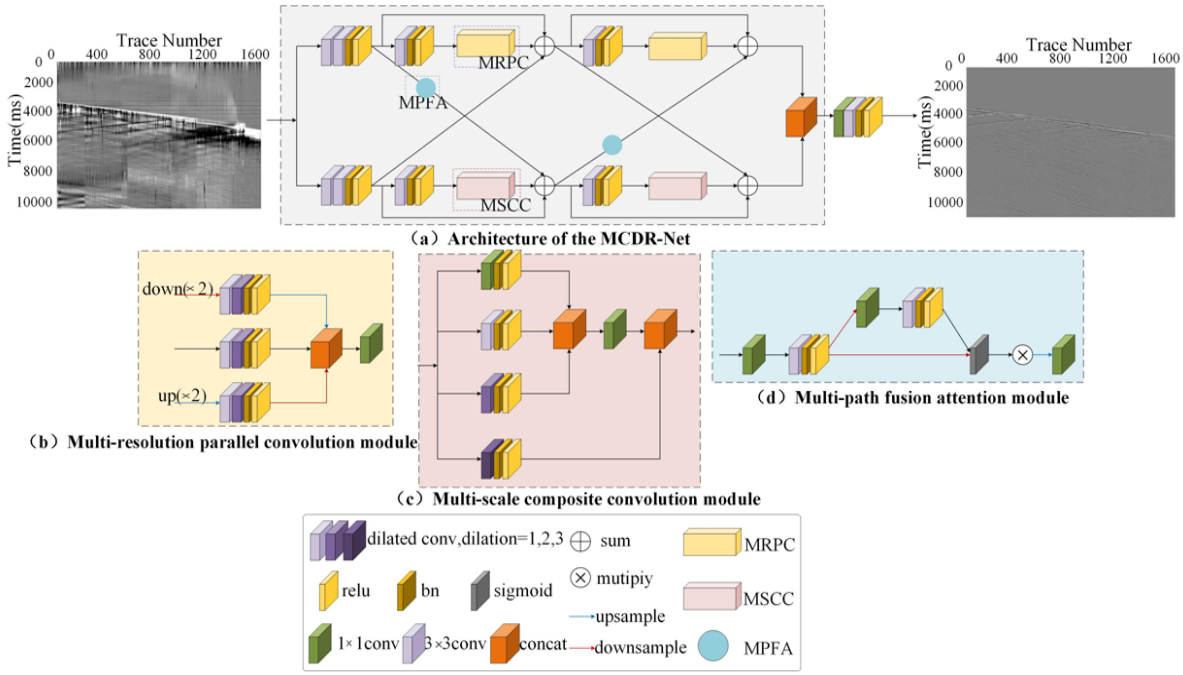

FIGURE 3. Architecture of the MCDR-Net: (a) Network architecture; (b) multi-resolution parallel convolution module; (c) multi-scale composite convolution module; (d) multi-path fusion attention module

through multi-scale composite convolution module (MSCC) (Figure 3(c)). The spatial-channel hybrid attention mechanism is used to fuse different features from the upper and lower branches through the multi-path fusion attention module (MPFA) (Figure 3(d)). As shown in Figure 3, the framework operates through three coordination mechanisms.

1) Dual-path feature extraction

The upper branch utilizes multi-resolution feature extraction through the most commonly used 3×3 convolutional layers, and combined with varying sampling operations (down-sample and up-sample) (Figure 3(b)) to preserve weak signals while reducing feature redundancy and effectively capturing multi-resolution information. At the same time, the lower branch implements multi-scale feature extraction using a hybrid structure: 1×1 convolutions and dilated convolutions with dilation rates of 1, 2, 3 are connected in parallel (Figure 3(c)). Among them, the 3×3 convolution kernel is mainly used to capture the basic local visual structure in the feature map and fine-tune the feature information. However, the 1×1 convolution is only computed in the channel dimension, which is very computationally inexpensive. The dilated convolution with dilation rates of 1, 2, 3 inserts dilation 0, 1, 2, respectively, between the standard convolution kernel elements, which is equivalent to expanding the receptive field without changing the size of the feature map [32] and effectively capturing richer information.

2) Attention-guided fusion

It is mainly divided into three stages. Firstly, part of the features from the upper branch are processed by the spatial-channel hybrid attention mechanism, where the weights are dynamically allocated according to the local SNR. Then, the focused feature is connected with the multi-scale features of the lower branch, and the fused information is refined by the second attention mechanism module. Finally, the refined features are cascaded with the remaining multi-resolution features from the upper branch to ensure the comprehensive utilization of the two branches, giving full attention to the useful information of the upper and lower branches.

3) Weak signal retention

The reserved enhancement of weak signals is mainly carried out from two aspects. The first aspect is based on dense residual connection, and the output of each fusion step is fed to the subsequent decoder layer through the residual connection as a priority input. At the same time, some shallow features are directly merged with the output of the final decoder through cross-layer concatenation, which also ensures that enough low-level details are retained in the denoising results.

3.1. **MRPC.** In the field of deep learning, data features with different resolutions may present different forms of expression. Therefore, the MRPC module is applied to the upper branch to extracting features at multiple resolutions. This module uses multiple paths for parallel processing.

1) The data is down-sampled with a sampling rate of 2, and then the spatial detail information at low resolution is retained by 3×3 convolution and 3×3 dilated convolution (dilation = 2).

2) The data is processed by 3×3 convolution and 3×3 dilated convolution (dilation = 2) to extract some local information at the same resolution.

3) The data is up-sampled with a sampling rate of 2, and then 3×3 convolution and 3×3 dilated convolution (dilation = 2) are used to cover a larger receptive field at high resolution to prevent weak signal loss.

Finally, the multi-level features from all three paths are concatenated and fused through a centralized processing mechanism. To avoid information loss during fusion, the output is further combined with the original input via residual connection. This design captures key multi-resolution information and enhances feature representation for the upper branch. The final output A of the MRPC module can be expressed as

$$A = Y_1(Concat(F_{down}(Y_3, Y_5), (Y_3, Y_5), F_{up}(Y_3, Y_5))) \tag{4}$$

where Y_i represents $i \times i$ convolution kernel, F_{down} represents the operation of down-sampling, and F_{up} represents the operation of up-sampling.

3.2. **MSCC.** Under the gradient dominance caused by high-amplitude noise in seismic data, weak signal features are suppressed during back propagation. To counteract this, the lower branch incorporates the MSCC module to efficiently extract multi-scale features by hierarchical processing to enhance detail preservation.

1) Local detail extraction: 1×1 convolution and dilated convolution kernels with dilation rates of 1, 2 are used to process data details separately and then concatenate them.

2) Global detail extraction: A dilated convolution kernel with a dilated rate of 3 is used to enlarge the receptive field to extract global information.

3) Cross-scale fusion: The outputs of all branches are concatenated to directly integrate local details (from dilation = 1, 2) and global context information (from dilation = 3). This parallel structure ensures the simultaneous capture of local and global information while maintaining computational efficiency. The final output B of the MSCC module can be expressed as

$$B = Concat(Y_1(Concat(Y_1, Y_3, Y_5)), Y_7) \tag{5}$$

where Y_i stands for $i \times i$ convolution kernel.

3.3. **MPFA.** In field seismic data under ultra-low SNR situation, traditional denoising methods are difficult to distinguish weak signals from noise due to frequency-domain interference between signal and noise components [33], which hinders the subsequent inversion and migration processes. In order to deal with this challenge, we develop the MPFA module which addresses this issue through a two-stage attention mechanism.

1) SNR guided weighting: The sigmoid function dynamically generates attention weights according to the local SNR to emphasize high SNR regions while suppressing noise-dominated regions.

2) Cross-branch refinement: The participating features are concatenated with the output of the lower branch.

The module improves the signal recovery ability of the network through the attention mechanism, reduces the influence of secondary features, and improves the robustness of the model by adaptively focusing on the key information in the seismic data. The final output C of the MPFA module can be expressed as

$$C = F_{up}(\sigma(F_{down}(Y_1, Y_3) \otimes (F_{down}(Y_1, Y_3), Y_1, Y_3)))Y_1 \tag{6}$$

where σ means the sigmoid function and $\otimes$ means multiplication.

4. Network Training.

4.1. Construction of datasets.

The training dataset integrates two principal components: a theoretically clean DAS-VSP datasets, as shown in Figure 4(a) generated through forward modeling methods (the specific parameters are shown in Table 1), along with a noise dataset constructed random intercepted noise blocks collected from field data. Extracting clean signals from a record that contains noise poses a significant challenge in the field of seismic exploration.

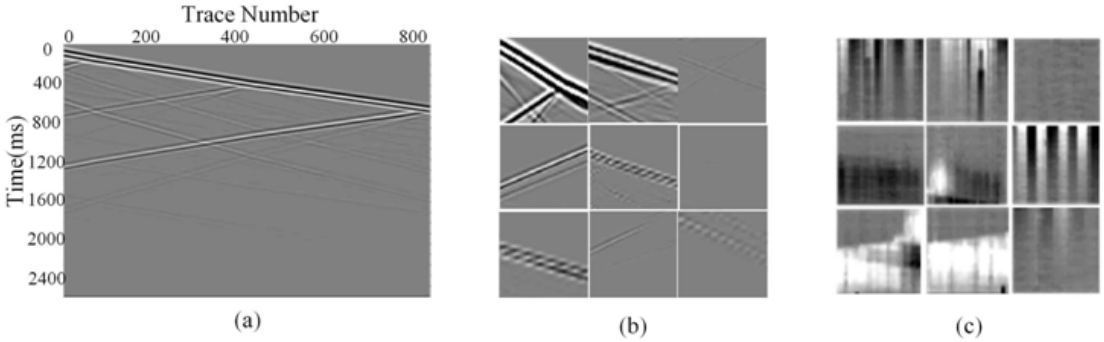

FIGURE 4. (a) Synthetic record; (b) samples of signal patches; (c) samples of noise patches

TABLE 1. Parameters related to forward modeling

Parameter	Set up
Seismic wavelet	Ricker wavelets
Fundamental frequency of wavelets	15-75 Hz
Propagation velocity	1200 m/s-2400 m/s
Medium density	1727.5 kg/m^3-2162 kg/m^3

This paper constructed 200 velocity models with varied velocities and densities, and computed 200 theoretical clean seismic records in total. Subsequently, a 64×64 sliding window captured the fragment of the clean records, as shown in Figure 4(b), resulting in clean signal blocks. Simultaneously, for enhancing training effectiveness, we removed the blocks with no signal and then normalized the rest by dividing them with the maximum absolute value. Then we built a clean signal training dataset $X = \{x_1, x_2, \ldots, x_n\}$ consisting of 20000 blocks.

The quality of the noisy datasets likewise influences the ultimate impact of the network during training. In order to enable the network to suppress different kinds of noise, multiple noise segments were extracted from the field seismic data, constituting a collection of noise. Our collection encompassed 3000 field noise records, and each comprises 20000 samples. Like the clean signal datasets, our approach involves utilizing a 64×64 sliding window for interception, as shown in Figure 4(c), and after normalization, the noise datasets $N = \{n_1, n_2, \ldots, n_m\}$ can be obtained.

To guarantee the ability of model in generalization capability, the clean signals and noise signals are randomly merged during training, thereby aligning with the field seismic data and forming the training datasets for denoising.

4.2. **Training process and experimental environments.** During the training phase, the batch size is set as 32, the initial learning rate is set to 0.005, and the Adam optimization algorithm is employed to optimize network parameters, to enhance the gradient descent process's effectiveness, the learning rate is recalibrated to 44% of its prior level after every 10 training epochs, with the training process ceased at the 60th epoch. As the training progress goes on, there is a steady reduction in training loss which indicates that the proposed method can effectively avoid the overfitting phenomenon. The specifics of network parameters are shown in Table 2.

TABLE 2. Configuration details of the MCDR-Net parameters

Hyper-parameter	Setting
Optimizer	Adam
Patch size, Batch size, Epoch	64×64, 32, 60
Learning rate range	$[10^{-3}, 10^{-5}]$
Total layers	39
Convolution kernel size	$1 \times 1 \times 64$, $3 \times 3 \times 64$, $5 \times 5 \times 64$

All training procedures and experimental evaluations are conducted on a PC that is equipped with an NVIDIA GeForce RTX 3060 GPU.

5. Experimental Results.

5.1. **Denoising on synthetic record.** Figure 5(a) shows a designed stratigraphic model that was employed to generate the clean synthetic seismic record which is shown in Figure 5(b). By adding the field noise as shown in Figure 5(c) into the clean synthetic record as shown in Figure 5(b), the synthesized record contains noise (Figure 5(d)) can be utilized as the input of network.

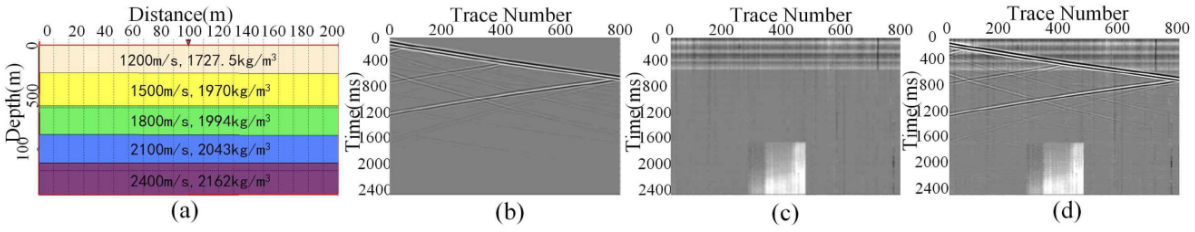

FIGURE 5. Generation of noisy record: (a) Stratigraphic model; (b) clean synthetic data; (c) field noise; (d) noisy record with an SNR of −5.1772 dB

We chose four widely used denoising algorithms as the competitive methods, including BPF, RPCA, DnCNN, and U-Net. In detail, passband of BPF is adjusted between 12-60 Hz, while loss function weight of RPCA is set as 0.006. The specific parameters of

TABLE 3. Network parameters of DnCNN and U-Net

Hyper-parameter	DnCNN	U-Net
Optimizer	Adam	Adam
Patch size, Batch size, Epoch number	64×64, 32, 60	64×64, 32, 60
Learning rate range	$[10^{-3}, 10^{-5}]$	$[10^{-3}, 10^{-5}]$
Total layers	17	27
Convolution kernel size	$3 \times 3 \times 64$	$3 \times 3 \times 64$, $3 \times 3 \times 128$, $3 \times 3 \times 256$, $3 \times 3 \times 512$

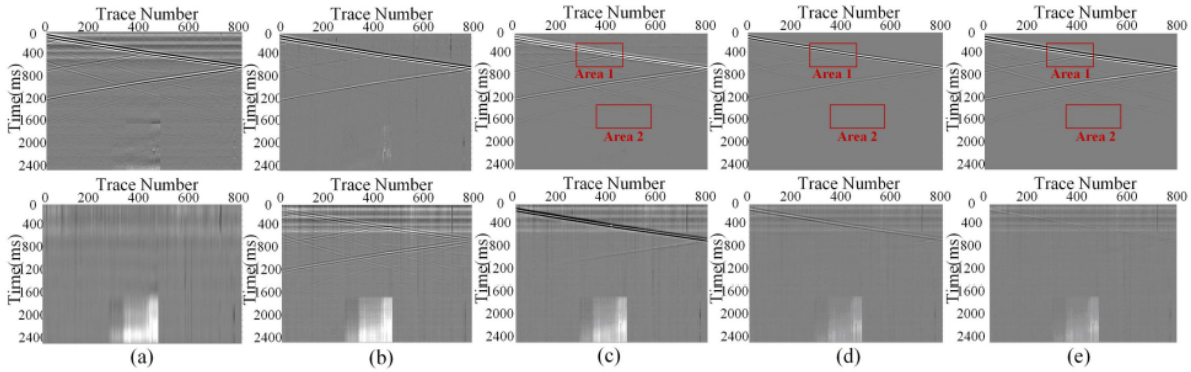

FIGURE 6. Performance of different denoising methods: (a)-(e) Denoising results and residual results obtained by BPF, RPCA, DnCNN, U-Net, and MCDR-Net, respectively

DnCNN and U-Net are shown in Table 3. Above methods were trained with identical training datasets, and are evaluated using the same testing datasets.

According to the noise reduction results of synthetic records presented in Figures 6(a) and 6(b), it is evident that spectral overlap between the pure signal and random noise exhibited substantial spectral overlap, which made it challenging for the BPF and the RPCA to effectively recover the signal. Although the CNN-based approaches demonstrated significant advantages over traditional methods in reducing background noise, the residual noise in DnCNN was pronounced (Figure 6(c)). Meanwhile, the signal recovery results of U-Net (Figure 6(d)) exhibited discontinuity in certain regions, with noticeable signal loss, as highlighted by the red box in the figure. Based on a comprehensive analysis, MCDR-Net outperformed the aforementioned methods about effectively reducing signal leakage and maintaining signal continuity while suppressing noise (Figure 6(e)).

In order to more clearly observe the specific differences, the red areas of the noise reduction results in Figure 6 are locally enlarged. From these magnified views, it is evident that the signal processed by MCDR-Net not only exhibits a significantly reduced noise level but also retains fine details effectively. In contrast, the signal processed by BPF in Figure 7(a) still contains residual high-amplitude noise components, while the signal processed by RPCA in Figure 7(b) shows reduced noise interference to some extent but continues to suffer from significant signal loss. Figure 7(c) and Figure 7(d) display the processing results of DnCNN and U-Net, respectively. The DnCNN processed signal remains noisy in certain areas, whereas the U-Net processed signal loses important details. These locally enlarged data further confirm the superiority of MCDR-Net in noise reduction and signal recovery.

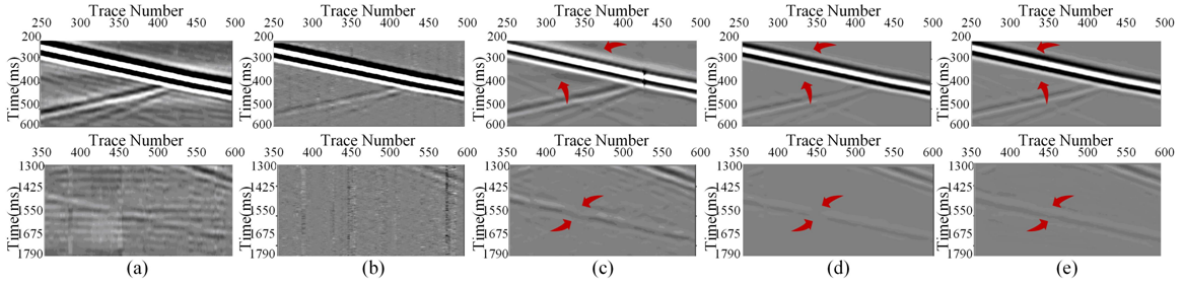

FIGURE 7. Comparison of the amplification local areas by different methods: (a)-(e) Magnified Area 1 (upper subgraph), magnified Area 2 (lower subgraph) from BPF, RPCA, DnCNN, U-Net, and MCDR-Net

5.1.1. *Analysis of results in time domain.* In order to compare the efficiency of different denoising techniques, this study employs global and local perspectives in time domain to verify the significant advantages of the proposed methods in noise suppression and signal recovery [34]. By selecting specific channel data and conducting quantitative waveform analysis to show the effects of different processing techniques.

Figure 8 presents a full time-domain comparison for the trace numbers of 0, 50, and 200, where a time range of 0-3 s is adopted. As shown in Figures 8(a), 8(b), and 8(c), the clean signal serves as a benchmark to evaluate the denoising performance of other methods. It is evident that their overall phase deviation is significant. In contrast, the global trend of the MCDR method closely aligns with the clean signal, with only minor amplitude differences in some regions, such as 1-2 seconds.

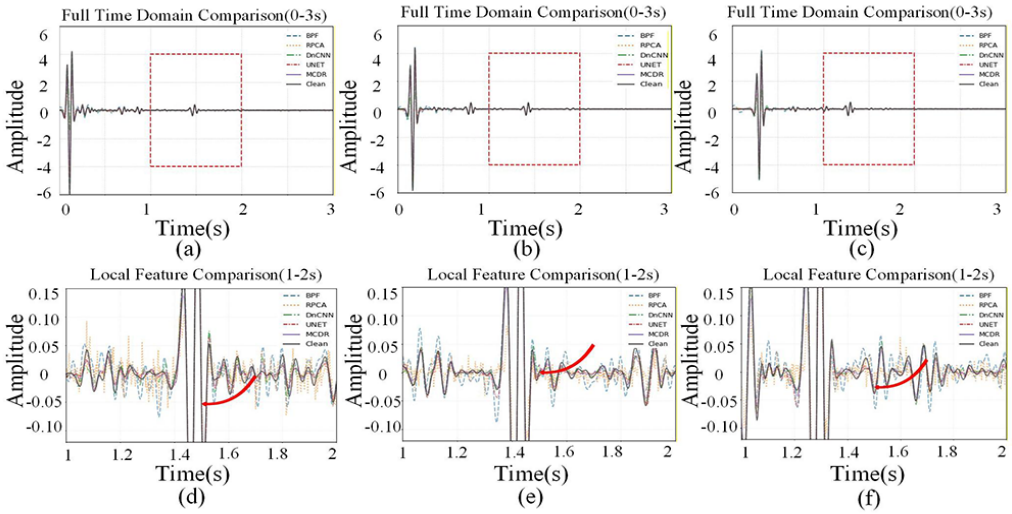

FIGURE 8. Time-domain comparison results for single trace: (a)-(c) Results of time comparison in trace number of 0, 50, 200 (0-3 s); (d)-(f) results of local comparison in trace number of 0, 50, 200 (1-2 s)

To more clearly observe the specific time domain variation trends of the denoising results for each method within the 1-2 s range, this specific region was expanded for further analysis, as shown in Figures 8(d), 8(e), and 8(f). In this enlarged region, other methods exhibit noticeable phase deviation, which somewhat diminish their denoising performance. However, the local fluctuations of MCDR show minimal phase deviation, with almost complete synchronization in the 1.4-1.6 s interval. Notably, around 1.5 s,

the signal is captured more accurately (as highlighted in the red arrow in the figure, the correlation coefficient is approximately 0.992), demonstrating that MCDR has significant advantages in detail preservation.

5.1.2. *Signal to noise ratio analysis.* In this study, SNR and root mean square error (RMSE) are employed as quantitative indicators to evaluate the performance of different methods. SNR is usually used to characterize signal purity, and RMSE is served as the core index to evaluate the prediction accuracy of the algorithm. Specifically, the formulae for calculating SNR and RMSE are defined shown below:

$$SNR = 10\lg\left(\sum_{i=1}^{X}\sum_{j=1}^{N} p(i,j)^2 \Big/ \sum_{i=1}^{X}\sum_{j=1}^{N}\left[\hat{p}(i,j) - p(i,j)\right]^2\right) \tag{7}$$

$$RMSE = \sqrt{\sum_{i=1}^{X}\sum_{j=1}^{N}\left[\hat{p}(i,j) - p(i,j)\right]^2 \Big/ XN} \tag{8}$$

where $\hat{p}(i,j)$ and $p(i,j)$ indicated the restored and clean signals, respectively. Detailed analysis results are shown in Table 4. Specifically, MCDR-Net provided over 21 dB increments for -10 dB records. In summary, MCDR-Net established the highest SNR improvement in the tests in this study, further confirming its effectiveness.

Table 4. Comparison of SNR and RMSE for different denoising methods

Original	BPF		RPCA		U-Net		DnCNN		MCDR-Net	
record/dB	SNR	RMSE	SNR	RMSE	SNR	RMSE	SNR	RMSE	SNR	RMSE
0	7.493	0.176	5.880	0.212	17.857	0.053	13.105	0.092	20.160	0.041
-2	5.500	0.221	3.951	0.264	15.841	0.067	11.127	0.116	17.214	0.057
-5	2.507	0.312	1.053	0.369	13.591	0.087	7.559	0.174	13.724	0.086
-7	0.510	0.393	-0.935	0.464	11.223	0.114	4.653	0.244	11.804	0.107
-10	2.488	0.555	-3.918	0.654	8.383	0.159	3.152	0.290	10.946	0.149

By calculating the local SNR under different noise reduction strategies and analyzing the resulting local SNR graphs, the performance of various noise reduction algorithms can be effectively evaluated, and the signal intensity distribution under different processing methods can be described.

In this study, a 5×5 sliding window was employed to divide the denoising result slices, enabling the calculation of the SNR for each slice based on the window size. Upon detailed observation, MCDR-Net in Figure 9(e) demonstrated superior SNR compared to the other four methods, particularly in regions with weak signal concentration. Specifically, as shown in Figure 9(a) and Figure 9(b), the lines in the figure are sparse and irregularly distributed, the contrast is weak, making it difficult to identify details in some areas, and the clarity of signal details remains insufficient. In Figure 9(c) and Figure 9(d), although the lines are relatively concentrated and exhibit clear contrast, with the overall SNR significantly improved compared to traditional methods, the line continuity in DnCNN and U-Net remains inadequate. In contrast, the yellow lines in MCDR-Net are extremely dense and regularly arranged, with a completely interference-free background. The contrast between the lines and the background reaches an optimal state, further verifying the exceptional performance of MCDR-Net in noise attenuation and signal retention.

5.1.3. *Analysis of results in frequency domain.* In the field of frequency domain analysis, this study investigated the signals and their differences when processed by different

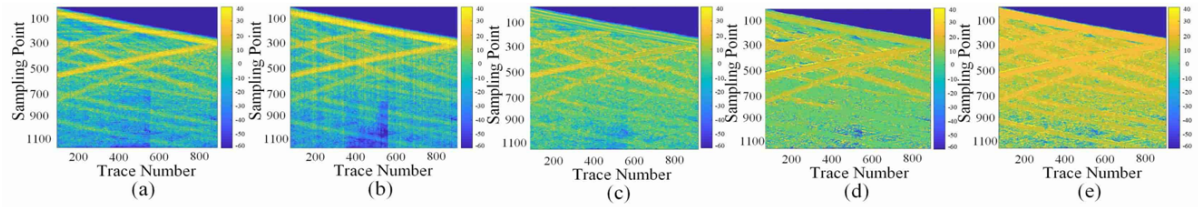

FIGURE 9. Local SNR comparisons for different processing results: (a)-(e) Local SNR outputs of BPF, RPCA, DnCNN, U-Net and MCDR-Net, respectively

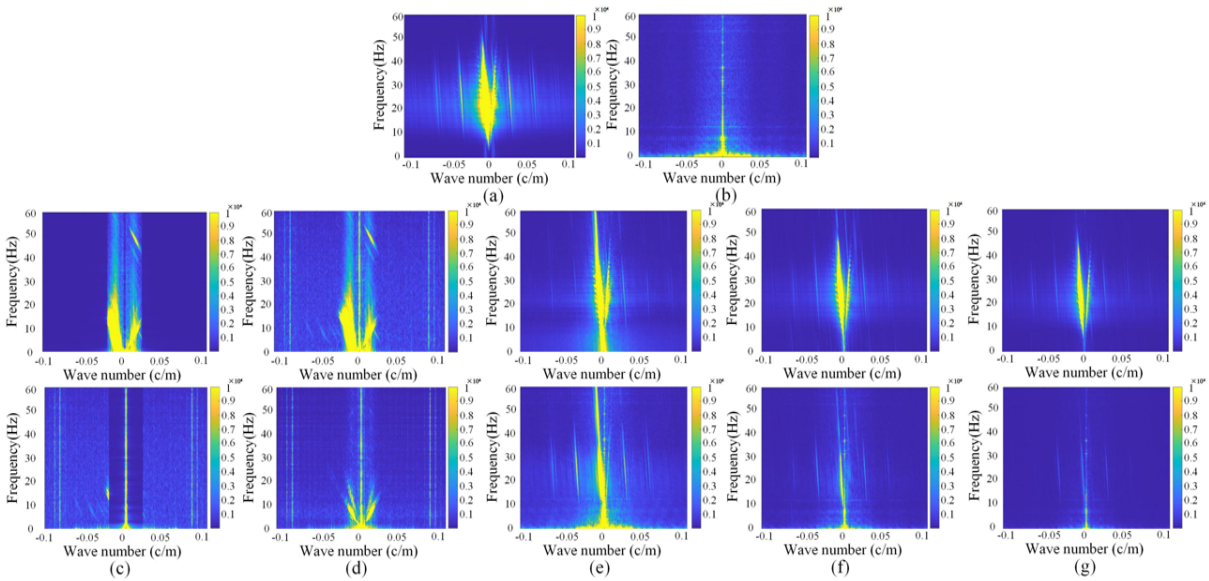

FIGURE 10. Results of denoising by different methods analyzed in F-K domain: (a) and (b) F-K spectra of pure record and added noise data; (c) F-K spectra of BPF denoising result and residual result; (d) F-K spectra of RPCA denoising result and residual result; (e) F-K spectra of DnCNN denoising result and residual result; (f) F-K spectra of U-Net denoising result and residual result; (g) F-K spectra of MCDR-Net denoising result and residual result

methods, as shown in Figure 10, aiming to evaluate the extent of signal leakage caused by each method in the spectrum. By comparing performance of different methods in spectral domain, the following observations were made.

As shown in Figure 10(a), the spectral structure serves as a denoising target, and subsequent models need to restore this structure as accurately as possible. In Figure 10(b), the noise component is clearly observed. In Figure 10(c), the BPF method demonstrated some suppression of low-frequency noise but introduced additional noise in the high-frequency region, and there is noticeable distortion, and residual noise remains evident. In Figure 10(d), the frequency distribution of the RPCA method is relatively scattered, and its noise suppression capability is weak. Artifacts are easily generated, particularly in the high-frequency region, resulting in damaged signal characteristics, a fuzzy state, and significant information leakage. In Figure 10(e), the frequency distribution of the DnCNN method is relatively concentrated, and its noise suppression effect is more significant than that of traditional methods. The signal characteristics are well-preserved, and most of the noise is effectively removed. As shown in Figure 10(f), the U-Net method exhibits a clear

frequency distribution and strong noise suppression capability, effectively removing noise while retaining signal characteristics with minimal noise residue. However, in contrast, as shown in Figure 10(g), the MCDR-Net method achieved superior overall performance. It not only excelled in noise suppression but also ensured the integrity of signal characteristics. The frequency distribution is highly concentrated, the signal characteristics are distinct, and the issue of signal distortion is avoided. Particularly in the low-frequency region, the main components of the signal can be clearly identified, and information leakage is minimal.

5.2. **Denoising on field record.** In this study, the noise reduction performance of MCDR-Net was evaluated using field DAS record. As shown in Figure 11(a), the raw seismic data is heavily contaminated by various noise, which significantly obscures the clarity of the effective signal. Figures 11(b)-(f) present the processing results of different noise reduction methods.

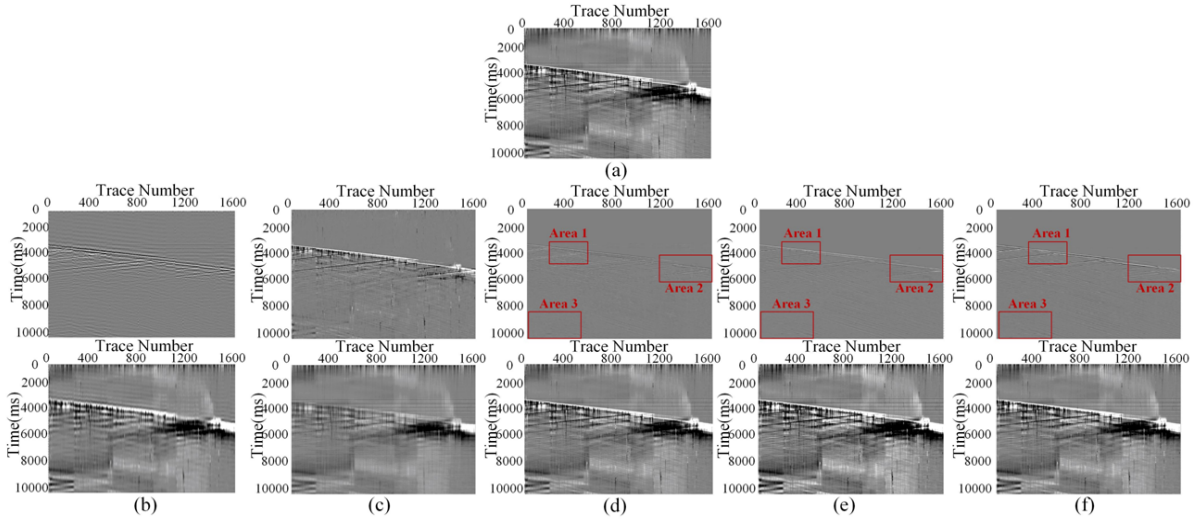

FIGURE 11. Denoising results of field seismic record: (a) Field seismic record; (b)-(f) denoising results and residual results obtained by BPF, RPCA, DnCNN, U-Net, and MCDR-Net

It is evident that the BPF (Figure 11(b)) and RPCA (Figure 11(c)) methods have limitations in separating signals and noise of similar frequencies. By comparing the processing results of different noise reduction algorithms, the results demonstrate that the signal recovered by MCDR-Net (Figure 11(f)) exhibits better continuity and is easier to identify. In contrast, DnCNN (Figure 11(d)) shows signal ambiguity in its results, while U-Net (Figure 11(e)) performs poorly in recovering some weak events, as illustrated in the red box in the figure.

To evaluate the efficiency of the above methods in signal recovery, the local details within the red boxes are magnified, as shown in Figure 12. Figure 12(a) and Figure 12(b) show the noise reduction results based on RPCA, which effectively removes part of the noise while retaining the main structural information of the data. However, some data details are lost in the process. In contrast, the CNN-based noise reduction method demonstrates better continuity and clarity in the denoised signal, making the reflected events easier to identify. Nevertheless, DnCNN shows limited effectiveness in processing horizontal and optical noise, as seen in Figure 12(c), where a small amount of noise remains. The U-Net method struggles to recover some weak signals, as shown in Figure 12(d). In Figure 12(e),

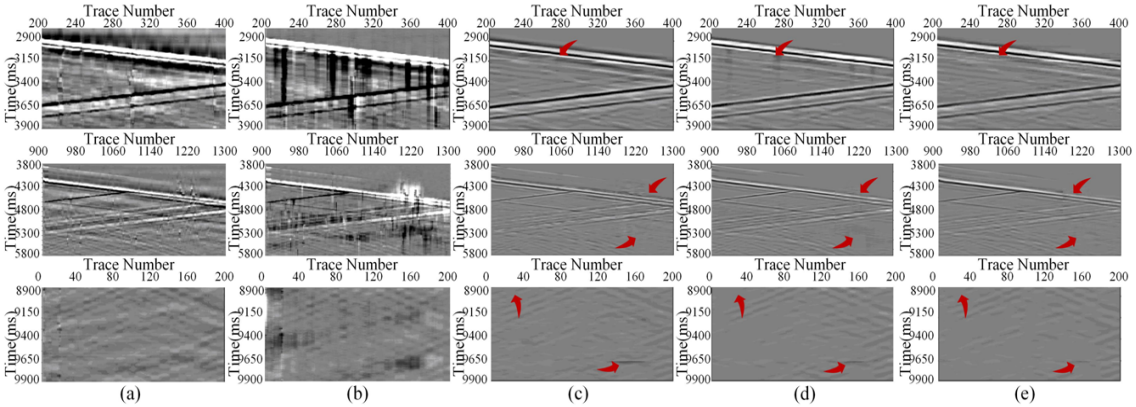

FIGURE 12. Comparison of local amplification by different methods: (a)-(e) Magnified Area 1 (upper subgraph), magnified Area 2 (middle subgraph) and magnified Area 3 (lower subgraph) from BPF, RPCA, DnCNN, U-Net, and MCDR-Net

compared to DnCNN and U-Net, MCDR-Net demonstrates superior performance in high-texture regions, which can preserve these details more effectively and excel in accurately identifying and recovering weak signals, as indicated by the red arrow in the figure.

6. **Discussion.** This section systematically examines the MCDR-Net's generalization capacity, while further evaluate its denoising efficacy against some contemporary frameworks.

6.1. **Analysis of generalization ability.** Generalization ability is a key index to measure the effectiveness of noise cancellation networks in practical application scenarios. In order to verify the generalization performance of MCDR-Net, different datasets were used for denoising. Figure 13(a) shows an example of desert data record with multiple noise types. During this process, we adjusted the pass-band range of the BPF to 0-15 Hz, while in RPCA, the weight of the loss function was set to 0.025. Figure 13(b) to Figure 13(f) show the output results obtained by different processing methods.

The original data (Figure 13(a)) contains a lot of noise, causing the effective signal to becomes blurred. The BPF method (Figure 13(b)) and the RPCA method (Figure 13(c)) can remove some of the noise, but the edges and details may still not be clear enough to accurately identify and analyze useful features. Compared to traditional methods, DnCNN (Figure 13(d)) and U-Net (Figure 13(e)) significantly reduce noise while preserving object details and edges. However, DnCNN, and U-Net methods proved to be slightly inadequate in detail recovery. However, MCDR-Net method (Figure 13(f)) combines multi-scale information, cross connection and dense residual connection to improve the denoising performance. While significantly reducing noise, MCDR method also retains data details and edge information.

In order to evaluate the denoising effect more accurately, this study carried out local magnification processing for the red box area marked in the figure. The magnified results were obtained by different processing methods are shown in Figure 14(b) to Figure 14(e). The analysis results showed that the BPF algorithm and RPCA method left more noise in the process of denoising, which makes the effective signals difficult to be clearly identified. Although DnCNN and U-Net models show high efficiency in noise removal, they demonstrated compromised signal fidelity characterized cannot realize complete signal reconstruction. In contrast, MCDR model demonstrated the ability to maintain signal continuity more effectively while maintaining low noise residue.

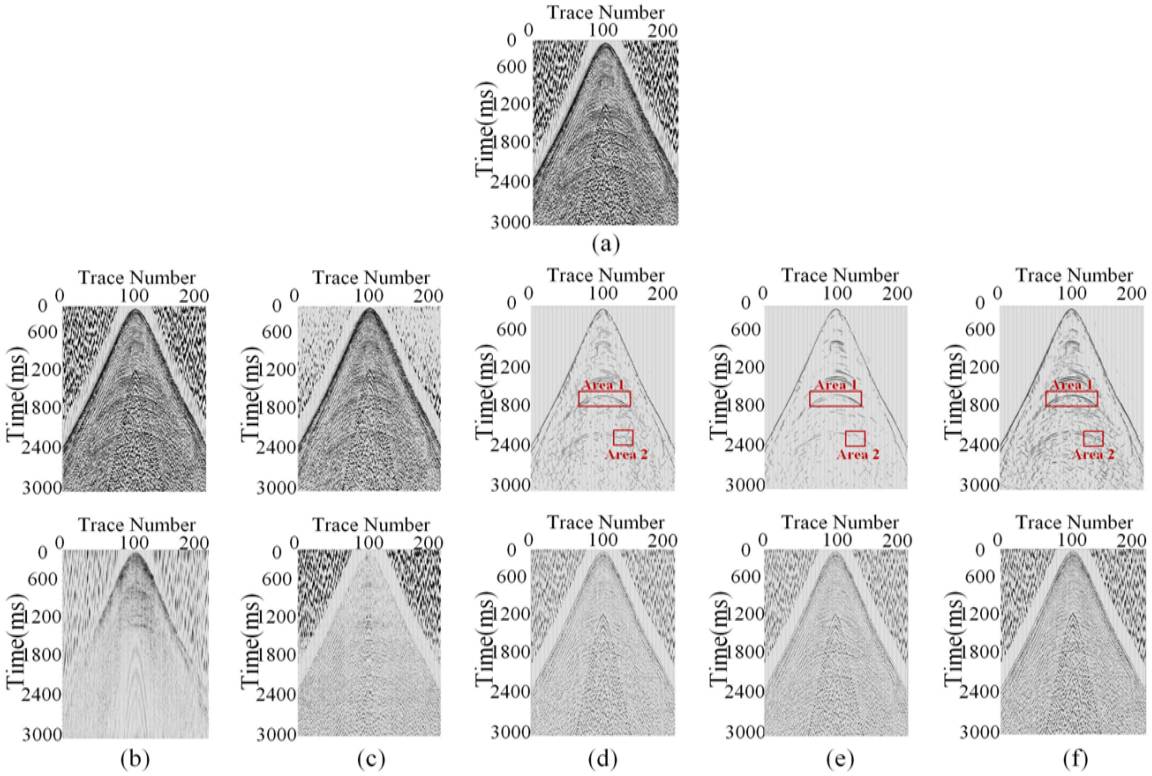

FIGURE 13. Generalizability analysis: (a) Field desert seismic data record; (b)-(f) denoising results and residual results obtained by BPF, RPCA, DnCNN, U-Net and MCDR-Net, respectively

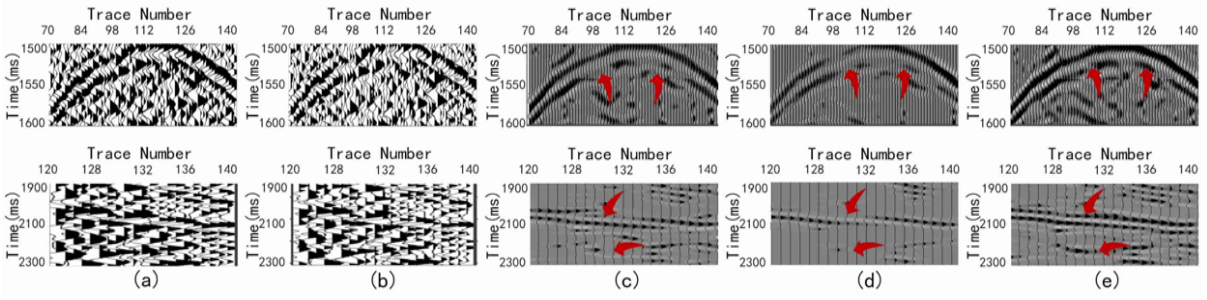

FIGURE 14. Comparison of local amplification by different methods: (a)-(e) Magnified Area 1 (upper subgraph) and Area 2 (lower subgraph) from BPF, RPCA, DnCNN, U-Net and MCDR-Net, respectively

6.2. **Comparison with some recent frameworks.** In signal and image processing, transformer-based techniques and self-supervised frameworks have garnered more interest lately. We compare MCDR-Net's performance objectively with two state-of-the-art methods: 1) self2self with weighted total variation (S2S-WTV) [35] and 2) swin transformer (ST) [36]. Every model uses the DAS dataset shown in Figure 15(a) and is trained using the same methods with optimized hyper-parameters. The denoising performance illustrated in Figure 15(b)-Figure 15(d) reveals critical distinctions. Specifically, S2S-WTV (Figure 15(b)) demonstrates limited effectiveness in reducing high-amplitude background artifacts, and it is difficult to achieve sufficient separation of effective signal and noise under strong noise conditions. ST (Figure 15(c)) demonstrates huge deficiencies in both signal preservation and residual noise suppression. However, MCDR-Net (Figure 15(d))

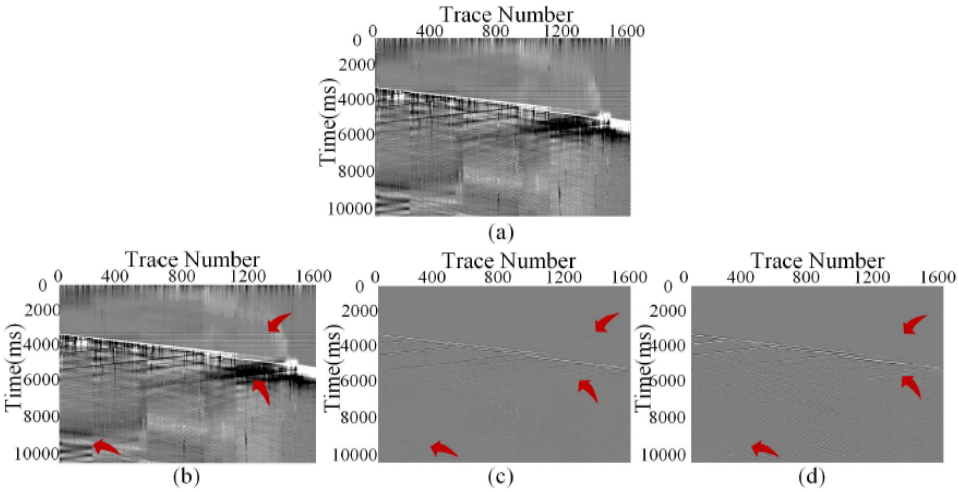

FIGURE 15. Comparison with recent frameworks of denoising results: (a) Field DAS record; (b)-(d) denoising results obtained by S2S-WTV, ST, and MCDR-Net, respectively

has almost no residual noise, while the recovered signal is clear and continuous (marked by the red arrows).

After in-depth analysis, the limited denoising performance of S2S-WTV and ST maybe derived from the following aspects. For one thing, S2S-WTV uses signal convolutional architecture and self-supervised learning strategy to train the denoising network, which may have difficulties in weak signal recovery. For another, ST model is generated by utilizing the global-scale information, which may degrade when processing denoising task. In contrast, MCDR-Net utilizes multi-scale features to refine the denoising models. Meanwhile, it also uses MPFA module to suppress weak noise interference at different fusion stages, aiming to improve the recovery of weak reflection signals. Therefore, we can get the point that MCDR-Net can provide better denoising performance, while the corresponding results also verify its effectiveness.

7. **Conclusion.** The study centered on the issue of intense random fluctuations in DAS-VSP, and an advanced MCDR-Net is proposed to proficiently reduce noise. This research demonstrates that a dual-branch network with dense cross residual links, integrated with a strategy for reusing information and an attention mechanism, adeptly achieves the reduction of random noise in seismic information.

In the training process, the theoretically pure DAS-VSP seismic datasets are constructed by using forward modeling method, and it is fused with the field noise data collected in the field survey to form training datasets which are suitable for network training. Compared with traditional noise processing techniques and other deep learning models, the experimental results show that MCDR-Net demonstrated effectiveness in suppressing noise, but also maintained the details and continuity of seismic signals, and significantly improved the SNR of data.

In addition, this study also combined the analysis in the time domain and frequency domain, and compared it with the local SNR graph, which further confirms the excellent performance of MCDR-Net in the field of signal processing. Compared to other technologies, MCDR-Net exhibits better robustness and generalization performance in processing complex seismic data, providing a more solid data foundation for subsequent imaging, inversion and interpretation tasks.

According to the comprehensive analysis, MCDR-Net, as an efficient background noise reduction technology, achieves remarkable progress in the denoising processing of DAS seismic data. In future development, this study will continue to explore more efficient multi-scale methods, in order to reduce the computational overhead, such as desiging lighweight models and applying in 3D seismic data process. Further enhance the processing accuracy of complicated seismic data.

REFERENCES

[1] F. Cheng, Photonic seismology: A new decade of distributed acoustic sensing in geophysics from 2012 to 2023, *Surveys in Geophysics*, vol.45, no.4, DOI: 10.1007/s10712-024-09840-0, 2024.

[2] A. Mateeva, J. Lopez, H. Potters, J. Mestayer, B. Cox, D. Kiyashchenko, P. Wills, S. Grandi, K. Hornman and B. Kuvshinov, Distributed acoustic sensing for reservoir monitoring with vertical seismic profiling, *Geophysical Prospecting*, vol.62, no.4, pp.679-692, DOI: 10.1111/1365-2478.12116, 2014.

[3] G. Bellefleur, E. Schetselaar, D. Wade, D. White, R. Enkin and D. R. Schmitt, Vertical seismic profiling using distributed acoustic sensing with scatter-enhanced fibre-optic cable at the Cu-Au New Afton porphyry deposit, *Geophysical Prospecting*, vol.68, no.1, pp.313-333, DOI: 10.1111/1365-2478.12828, 2020.

[4] H. Z. Wang, J. Lin, X. T. Dong and D. D. Jiang, Signal recovery and noise suppression of the ocean-bottom cable P-component data based on improved dense convolutional network, *Geophysical Prospecting*, vol.72, no.4, pp.1498-1521, DOI: 10.1111/1365-2478.13426, 2024.

[5] R. A. Stein and N. R. Bartley, Continuously time-variable recursive digital band-pass filters for seismic signal processing, *Geophysics*, vol.48, no.6, pp.702-712, DOI: 10.1190/1.1441500, 1983.

[6] L. L. Canales, Random noise reduction, *SEG Technical Program Expanded Abstracts*, 329, DOI: 10.1190/1.1894168, 1984.

[7] S. Y. Yuan, Y. Liu, Z. Zhang, C. M. Luo and S. X. Wang, Prestack stochastic frequency-dependent velocity inversion with rock-physics constraints and statistical associated hydrocarbon attributes, *IEEE Geoscience and Remote Sensing Letters*, vol.16, no.1, pp.140-144, DOI: 10.1109/LGRS.2018.2868831, 2019.

[8] N. H. Liu, J. H. Gao, B. Zhang, Q. Wang and X. D. Jiang, Self-adaptive generalized S-transform and its application in seismic time-frequency analysis, *IEEE Transactions on Geoscience and Remote Sensing*, vol.57, no.10, pp.7849-7859, DOI: 10.1109/TGRS.2019.2916792, 2019.

[9] R. Tao, Y. L. Li and Y. Wang, Short-time fractional Fourier transform and its applications, *IEEE Transactions on Signal Processing: A Publication of the IEEE Signal Processing Society*, vol.5, DOI: 10.1109/TSP.2009.2028095, 2010.

[10] M. Cheng, S. P. Lu, X. T. Dong and T. Zhong, Multi scale recurrent-guided denoising network for distributed acoustic sensing-vertical seismic profile background noise attenuation, *Geophysics*, vol.88, no.1, pp.WA201-WA217, DOI: 10.1190/geo2022-0269.1, 2022.

[11] Z. Zheng, S. Ahn and D. Chen, Applications of wavelet transform for analysis of freeway traffic: Bottlenecks, transient traffic, and traffic oscillations, *Transportation Research Part B: Methodological*, vol.45, no.2, pp.372-384. DOI: 10.1016/j.trb.2010.08.002, 2011.

[12] J. P. A. Sanchez, O. C. Alegria, M. V. Rodriguez et al., Detection of ULF geomagnetic anomalies associated to seismic activity using EMD method and fractal dimension theory, *IEEE Latin America Transactions*, vol.15, no.2, pp.197-205, DOI: 10.1109/TLA.2017.7854612, 2017.

[13] F. Qu, Q. Jiang, G. Jin, Y. Wei and Z. Wang, Noise cancellation for continuous wave mud pulse telemetry based on empirical mode decomposition and particle swarm optimization, *Journal of Petroleum Science and Engineering*, vol.200, no.1, 108308, DOI: 10.1016/j.petrol.2020.108308, 2020.

[14] M. Bekara and M. V. D. Baan, Random and coherent noise attenuation by empirical mode decomposition, *Geophysics*, vol.74, no.5, pp.V89-V98, DOI: 10.1190/1.3157244, 2011.

[15] Y. K. Chen and S. Fomel, EMD-seislet transform, *Geophysics*, vol.83, no.1, pp.27-32, DOI: 10.1190/GEO2017-0554.1, 2017.

[16] Z. K. Taha, J. K. S. Paw, R. S. Ali, Y. C. Tak and T. S. Kiong, Federated unsupervised and semi-supervised transfer learning for addressing scarcity and imbalanced human activity recognition, *International Journal of Innovative Computing, Information and Control*, vol.21, no.5, pp.1415-1434, DOI: 10.24507/ijicic.21.05.1415, 2025.

[17] Y. Liu, C. P. Zhang et al., Deduction of the transformation regulation on voltage curve for lithium-ion batteries and its application in parameters estimation, *eTransportation*, vol.12, 100164, DOI: 10.1016/j.etran.2022.100164, 2022.
[18] Z. Y. Ma, Z. Q. Zheng, J. W. Wei, Y. Yang and H. T. Shen, Instance-dictionary learning for open-world object detection in autonomous driving scenarios, *IEEE Transactions on Circuits and Systems for Video Technology*, vol.34, no.5, pp.3395-3408, DOI: 10.1109/TCSVT.2023.3322465, 2024.
[19] H. T. Ma, J. Yan and Y. Li, Low-frequency noise suppression of desert seismic data based on variational mode decomposition and low-rank component extraction, *IEEE Geoscience and Remote Sensing Letters*, vol.17, no.2, pp.337-341, DOI: 10.1109/LGRS.2019.2919795, 2020.
[20] T. M. V. Suryanarayana and P. B. Mistry, Principal component analysis in transfer function, in *Principal Component Regression for Crop Yield Estimation. SpringerBriefs in Applied Sciences and Technology*, Springer, Singapore, DOI: 10.1007/978-981-10-0663-0_2, 2016.
[21] X. Y. Liu, X. H. Chen, J. Y. Li and Y. K. Chen, Nonlocal weighted robust principal component analysis for seismic noise attenuation, *IEEE Transactions on Geoscience and Remote Sensing*, vol.59, no.2, pp.1745-1756, DOI: 10.1109/TGRS.2020.2996686, 2021.
[22] H. M. Wu et al., The improved wavelet denoising scheme based on robust principal component analysis for distributed fiber acoustic sensor, *IEEE Sensors Journal*, vol.23, no.19, pp.22944-22951, DOI: 10.1109/JSEN.2023.3305532, 2023.
[23] Z. Kasina, The analysis of the effectiveness of the seismic noise attenuation by means of Karhunen-Loeve (K-L) transform, *Geologia*, vol.36, no.2, pp.203-221, DOI: 10.7494/GEOL.2010.36.2.203, 2011.
[24] K. Zhang et al., Beyond a Gaussian denoiser: Residual learning of deep CNN for data denoising, *IEEE Transactions on Data Processing*, vol.26, no.7, pp.3142-3155, DOI: 10.1109/tip.2017.2662206, 2017.
[25] C. M. Manu and K. G. Sreeni, GANID: A novel generative adversarial network for image dehazing, *The Visual Computer*, pp.1-14, DOI: 10.1007/s00371-022-02536-9, 2022.
[26] Y. X. Zhao et al., Low-frequency noise suppression method based on improved DnCNN in desert seismic data, *IEEE Geoscience and Remote Sensing Letters*, DOI: 10.1109/LGRS.2018.2882058, 2018.
[27] W. D. Li, H. Liu and J. Wang, A deep learning method for denoising based on a fast and flexible convolutional neural network, *IEEE Transactions on Geoscience and Remote Sensing*, vol.60, pp.1-13, DOI: 10.1109/TGRS.2021.3073001, 2022.
[28] O. Ronneberger, P. Fischer and T. Brox, U-Net: Convolutional networks for biomedical data segmentation, *Medical Image Computing and Computer-Assisted Intervention – MICCAI 2015*, DOI: 10.1007/978-3-319-24574-4_28, 2015.
[29] T. Zhong, M. Cheng, X. T. Dong, Y. Li and N. Wu, Seismic random noise suppression by using deep residual U-Net, *Journal of Petroleum Science and Engineering*, 109901, DOI: 10.1016/j.petrol.2021.109901, 2022.
[30] K. Suayngam, R. Prasertpong, W. Nakkhasen, P. Julatha and A. Iampan, Pythagorean fuzzy sets: A new perspective on IUP-algebras, *International Journal of Innovative Computing, Information and Control*, vol.21, no.2, pp.339-357, DOI: 10.24507/ijicic.21.02.339, 2025.
[31] T. Zhong, M. Cheng, S. P. Lu, X. T. Dong and Y. Li, RCEN: A deep-learning-based background noise suppression method for DAS-VSP records, *IEEE Geoscience and Remote Sensing Letters*, vol.19, pp.1-5, DOI: 10.1109/LGRS.2021.3127637, 2021.
[32] T. Zhong and Y. Song, MPGA-Net: A multi-path guided attention network for desert seismic noise attenuation, *International Journal of Innovative Computing, Information and Control*, vol.21, no.3, pp.667-682, DOI: 10.24507/ijicic.21.03.667, 2025.
[33] T. Zhong, Z. Cong, X. Q. Tong, S. Q. Dong, S. P. Lu and X. T. Dong, Mutual-guided scale-aggregation denoising network for seismic noise attenuation, *Computers and Geosciences*, vol.191, DOI: 10.1016/j.cageo.2024.105682, 2024.
[34] Z. Chen, Time-domain and frequency-domain approaches to identification of bridge flutter derivatives, *Frontiers of Structural and Civil Engineering*, vol.3, no.2, pp.173-179, DOI: 10.1007/s11709-009-0034-1, 2009.
[35] Z. Xu, Y. Luo, B. Wu et al., S2S-WTV: Seismic data noise attenuation using weighted total variation regularized self-supervised learning, *IEEE Transactions on Geoscience and Remoter Sensing*, vol.61, DOI: 10.1109/TGRS.2023.3268554, 2023.
[36] Z. D. Xie et al., Self-supervised learning with swin transformers, *arXiv Preprint*, arXiv: 2105.04553v2, 2021.

Author Biography

Tie Zhong received the B.S., M.S., and Ph.D. degrees in Communication Engineering from Jilin University, China, in 2006, 2008 and 2016, respectively. He is currently an Associate Professor in the Key Laboratory of Modern Power System Simulation and Control and Renewable Energy Technology, Ministry of Education, and Department of Communication Engineering, Northeast Electric Power University, China. His research interests include modern signal processing techniques, weak signal process theory, and intelligent information processing.

Fanchao Xue received the B.S. degree in Communication Engineering from Northeast Electric Power University, China, in 2021. She is pursuing the M.S. degree in Information and Communication Engineering, Northeast Electric Power University. Her research interests include digital signal processing and seismic data denoising.

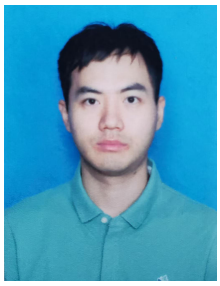

Shiqi Dong received the B.S., M.S., and Ph.D. degrees in Communication Engineering from Jilin University, China, in 2016, 2018 and 2021, respectively. He is currently an Associate Professor in the Key Laboratory of Modern Power System Simulation and Control and Renewable Energy Technology, Ministry of Education, and Department of Communication Engineering, Northeast Electric Power University, China. His research interests include artificial intelligence signal and image processing, seismic inversion and imaging.